Tellus (2007), 59A, 571–590
Printed in Singapore. All rights reserved

TELLUS

REVIEW ARTICLE

Large-scale, free Rossby waves in the atmosphere—an update

By ROLAND A. MADDEN*, *National Center for Atmospheric Research, Boulder, CO 80307-3000, USA*

(Manuscript received 19 November 2006; in final form 14 May 2007)

ABSTRACT

The existence of free, or normal mode Rossby waves has been known for 50 yr. Studies have indicated that they can affect the large-scale flow in important ways; nevertheless there has been little written on them during the last decade. Here, evidence of their presence in a 40-yr record of NCEP/NCAR Reanalysis data is presented. It provides a starting point from which other published observations based on varying data sets are summarized. In addition, literature pointing to their possible effects is summarized. This update is submitted in the hopes that it will reinvigorate interest that can increase our understanding of variations in the large scales.

1. Introduction

In the very first issue of this Journal, Rossby considered how 'planetary waves' would propagate the influence of a source point. Rossby says, 'the term planetary waves is here applied to those quasi-horizontal atmospheric motions whose shape, wavelength and displacements are controlled by the variation of the Coriolis parameter with latitude...' (Rossby, 1949). Rossby's planetary waves are now most often referred to as Rossby waves after his famous 1939 paper (Rossby et al., 1939). Here, we briefly outline the theory, give evidence for the existence of Rossby waves in a 40-yr record of NCEP/NCAR Reanalysis data, and review some of their reported effects.

While the 1939 paper must be credited with introducing Rossby waves to the mainstream meteorology of the time, their theoretical treatment goes back to the early-19th century and the work of LaPlace who studied waves in an ocean of uniform depth and in an isothermal atmosphere on rotating spheres. LaPlace derived the Tidal Equations. Most important intervening work was probably that of Hough (1898), after which the functions that describe the horizontal structures of the waves are named and Margulis (1893). Longuet-Higgins (1968) calculated many Hough functions to show the latitudinal dependence of free waves of the Tidal Equations. There are two kinds of wave solutions: waves of the First Class which depend on gravity, and waves of the Second Class which depend on the Earth's rotation. It is the dynamics of these second waves that Rossby (Rossby et al., 1939) isolated, and it is these that are of singular importance in meteorology. Platzman (1968) has provided an excellent review of the Rossby wave.

In a continuing study of large-scale Rossby waves, their existence and their effects, we have been examining a 40-yr record of NCEP/NCAR Reanalysis data (Kalnay et al., 1996). For background, the theory of Rossby waves is outlined in Section 2. The data and analysis method are discussed in Section 3. Evidence of Rossby waves in these data, related in Section 4, provides a framework for a synthesis of this and other already published work on the subject, which is presented in Section 5.

Most convincing early evidence of the existence of Rossby waves also appeared in *Tellus* (Eliasen and Machenhauer, 1965, 1969). Probably the waves that have received the most attention are the zonal wavenumber one, '5-Day Wave' (Deland, 1964), the '10-Day Wave' (Hirooka and Hirota, 1985) and the '16-Day Wave' (Madden, 1978). The Branstater–Kushnir wave (Branstater, 1987; Kushnir, 1987) might be a candidate for the wavenumber one 25-d free Rossby wave, but in their study of the effects of a wavy, stationary background flow Branstater and Held (1995) conclude that it is more likely an unstable mode. There is, however, some evidence that a 25-d, free Rossby wave can be identified although its structure, and that of other slow moving modes, are distorted by the background flow.

There have been reviews of these and other early observations (Madden, 1979; Salby, 1984) so, in Section 5 here, we limit our review of observational results to those published in the last couple of decades. Finally, we review reported effects of the waves on some time variations in the large-scale circulation,

*Correspondence.
e-mail: ram@ucar.edu
DOI: 10.1111/j.1600-0870.2007.00257.x

their presence in numerical models, and their possible excitation mechanisms in Sections 6–8.

2. Theory of free Rossby waves

Rossby's wave equation (1939) is:

$$c = U - \beta L^2/4\pi^2, \tag{1}$$

where c is the wave phase speed, U is the background west-to-east wind, β is the rate of change of the Coriolis force ($2\Omega\sin\varphi$, Ω is the rotation rate of the Earth) in the south-to-north direction, φ is latitude, and L the wavelength. This simple equation allowed weather forecasters of the time to make quantitative estimates of wave speeds to replace what had primarily been qualitative forecasting methods. The model for (1) is non-divergent waves on a plane. Equation (1)'s simplicity captures the basic dynamics of Waves of the Second Class. Its basis is the conservation of absolute vorticity and the resulting exchange from planetary to relative vorticity in flow from the north and the opposite exchange in flow from the south.

Haurwitz (1940) dropped the geometry of the plane for a more realistic spherical geometry. He maintained the non-divergent assumption and showed in that case that horizontal structures for the stream function, ψ, of the waves were associated Legendre polynomials. Associated Legendre polynomials are characterized by a zonal wavenumber, $\boldsymbol{s}$, and a meridional index, $\mathbf{l}$. The difference, $\boldsymbol{l} - \boldsymbol{s}$, gives the number of their zero crossings between the North and South Poles. The dotted lines in Fig. 1 present the latitudinal dependence of these functions for the largest scale waves. These then define horizontal structures that we would expect to find for ψ if the atmosphere were non-divergent and there were no background winds. Waves that are antisymetric about the equator in ψ are termed 'symmetric modes' because perturbations in their pressure are symmetric.

The non-divergent case does not provide realistic estimates for the periods or propagation speed of the large-scale, free Rossby waves. For more realism, wave periods are given by the eigenvalues of the LaPlace Tidal Equations which allow for divergence. They, along with the horizontal structures (eigenvectors), which are called Hough functions can be found in Longuet-Higgins (1968) for various equivalent depths. The equivalent depth is the separation constant between horizontal and vertical dependence of the waves and in the case of free waves (no forcing), the vertical structure equation gives an equivalent depth for the atmosphere near 8–10 km (see Diky, 1965; Lindzen, 1967). The solid lines in Fig. 1 show the latitudinal structure of Hough function depictions of ψ for a 10 km equivalent depth (after Kasahara, 1976). Hough functions are sums of spherical harmonics whose latitudinal dependence are associated Legendre polynomials and whose longitudinal dependence are sinusoids.

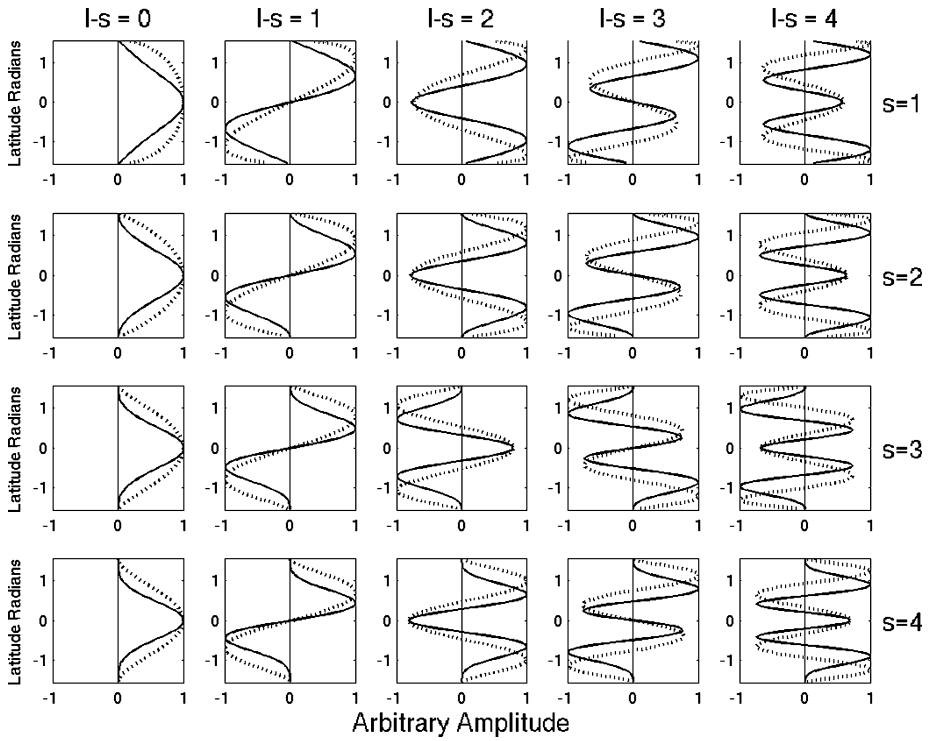

Fig. 1. Dotted lines are Associated Legendre Polynomials that give the theoretically predicted latitudinal dependence of ψ (stream function) of free Rossby waves in non-divergent flow (Haurwitz, 1940). Solid lines are the Hough function depictions of the latitudinal dependence of ψ predicted by the LaPlace Tidal Equations. Each row is for a different zonal wavenumber, $\boldsymbol{s}$, and each column is for a different meridional index, $\boldsymbol{l} - \boldsymbol{s}$. Hough functions are after Kasahara (1976).

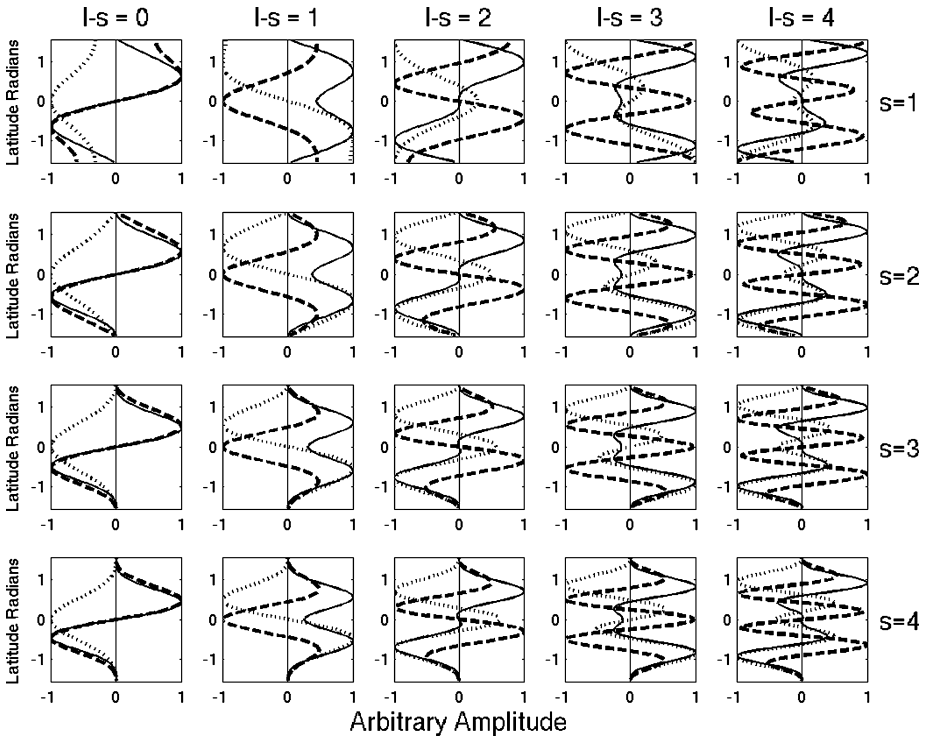

Fig. 2. Hough function depictions of the latitudinal structure of u (dashed), v (dotted) and Z (solid) for zonal wavenumber s (rows), and meridional index $l - s$ (columns). Hough functions are after Kasahara (1976). Each variable is normalized to a maximum amplitude of one.

For the largest scale waves, all coefficients except those for the leading terms are close to zero (Diky and Golitsyn, 1968). As a result, the Hough function depictions of ψ are similar to those of the single associated Legendre polynomial depictions (dotted lines in Fig. 1). Figure 2 shows the latitudinal structure of the Hough Function depictions of Z (geopotential height—solid), u (zonal wind—dashed) and v (meridional wind—dotted) for the largest scale waves and a 10 km equivalent depth (all after Kasahara, 1976).

The vertical structure of the free Rossby waves is that of the Lamb Wave (Lamb, 1932, p. 548; Lindzen, 1967; Salby, 1984). Their energy decays exponentially with height, but because of the density decrease, Z, u and v perturbations actually grow. They are equivalent barotropic; that is there is no slope with height, and thus, they are sometimes referred to as external Rossby waves (Geisler and Dickinson, 1975). Comparisons of the observed vertical structures with those of the Lamb Wave for some modes are shown in Madden (1978), Speth and Madden (1983), Hirota and Hirooka (1984), Hirooka and Hirota (1985), Venne (1989) and Hirooka (2000).

Realistic winds can alter wave propagation speed and local periods. Kasahara (1980) studied the effects of mean zonal flows in solutions of the linearized Tidal Equations. Resulting periods taken from Kasahara's Table 1 for December–January–February average winds are shown here in Table 1. Free waves designated in the Table are all westward propagating. Kasahara reported

Table 1. Theoretically predicted periods (d) of large-scale free Rossby waves in the presence of December–January–February averaged winds estimated by Kasahara (1980). Each row is for a different zonal wavenumber, s and each column is for a different meridional index, $l - s$

Periods (d) Divergent Rossby waves on a Sphere DJF winds (Kasahara, 1980: JAS)					
$s \backslash l - s$	0	1	2	3	4
1	1.20	4.85	9.91	18.39	28.08
2	1.71	3.84	7.27	14.23	21.47
3	2.30	4.28	7.40	13.65	–
4	2.90	5.21	8.20	13.55	–

Note: s = zonal wavenumber l = meridional index.

no values for $s = 3$ and 4 and $l - s = 4$ because the relative smallness of those waves' phase velocities in comparison with the background winds renders them part of a continuous spectrum rather than as discrete waves. Branstator and Held (1995), linearized the non-divergent barotropic vorticity equation, not about a zonal mean state, but about a zonally asymmetric, wavy basic state and presented evidence to support the likely existence of almost the same modes. They concluded that waves of $s = 1$ and 2 and $l - s < 4$ could exist as discrete, identifiably modes. They reached a similar conclusion for $s = 3$ and 4 and

$l - s < 2$. Salby (1981a,b) used a linearized general circulation model and reported similar results to those of Table 1 for comparable modes. He quantified the frequency spreading about the expected frequency due to background winds. He pointed out that frequencies of the slower moving, smaller scale modes can overlap, making their identification difficult or impossible. He concluded that at least those modes with $l < 4$ should be easily identifiable in the data.

Kasahara (1980) and Ahlquist (1982) found that horizontal structures of the largest waves are not badly affected by realistic winds at 500 hPa beyond asymmetries favouring the winter hemisphere for modes with larger l values. Salby (1981b) showed similar results held throughout the troposphere (lowest two scale heights).

In summary, these studies suggest that waves of small s and l should be detectable in observations despite the complicating factors associated with the average background flow. The horizontal structures of Figs. 1 and 2, and the periods of Table 1 provide guides in a search for these large-scale, free Rossby waves. Because our data are stream functions, the theoretical prototypes for horizontal structures are the Hough function depictions of ψ shown in Fig. 1.

Before leaving this section it is important to mention that waves with the very largest latitudinal scale, or the gravest free modes, are special cases called Mixed Rossby-Gravity (MRG) waves. They get their name because they obey the dispersion relation for gravity waves in fluids of small equivalent depth and that for Rossby waves in fluids of large equivalent depth (e.g. see eigenfrequencies presented by Longuet-Higgens, 1968). The equivalent depth of about 10 km is of intermediate size. A MRG wave prominent in the literature is the $s = 3, l = 3$, '2-Day Wave', that is frequently observed in the stratosphere and higher (Salby, 1981c).

3. Data and analysis method

3.1. Data

The data set we study consist of 300 hPa maps of ψ computed from the NCEP/NCAR Reanalysis at 00 and 12 UTC for the 40-yr period 1958–1997. There are 29 220 total maps. Data were projected onto spherical harmonics whose latitudinal dependence are associated Legendre polynomials and whose longitudinal dependence are sinusoids. These spherical harmonic projections are convenient since, as discussed above, theoretical expectations for ψ of a normal mode are sums of them and, for waves studied here, closely resemble single harmonics. These data have been studied by Branstator and colleagues (e.g. Branstator and Fredricksen, 2003).

Only spherical harmonics of order 1–4 (zonal wavenumbers, $s = 1$, 2, 3 and 4) and degree s through $s + 5$ were retained. A smooth seasonal variation was removed. The smooth seasonal variation was estimated by first computing the 40-yr average amplitude of each spherical harmonic at 00 and 12 UTC for each day of the year. Second, the resulting two 365 daily averages were Fourier transformed, the first four annual waves were retained, and their inverse transform computed. Data with these smooth seasonal variations removed will be referred to as 'basic' although it should be remembered that they have been filtered in space by retaining only the largest spatial scales and in time by removing the smooth seasonal variation. Leap days were treated as 28 February in removing the seasonal cycle.

3.2. Method of analysis

Daley and Williamson (1985) cautioned that even local disturbances that are confined to one hemisphere will project onto the global horizontal structures like those of Figs. 1 and 2. That is, projecting data onto a pre-selected structure will give an amplitude for that structure whether or not it has any physical meaning. To avoid prejudicing the results of his analysis of Rossby waves in this way, Venne (1989) computed Complex Empirical Orthogonal Functions (CEOFs), to let the data define wave structures. Here we follow his lead and look initially for the real (not complex) Empirical Orthogonal Functions (EOFs) of our data that most resemble theoretically predicted latitudinal structures and that propagate westward as predicted. The spherical harmonic amplitudes of the six retained latitudinal structures ($l = s \ldots s + 5$) for a single zonal wavenumber, s, were first subjected to an eigenvector analysis. EOFs or eigenvectors of a 12×12 covariance matrix based on all six retained degrees of the spherical harmonics of each zonal wavenumber were determined using the EIG routine of MATLAB. Table 2 is presented to illustrate the 12 spherical harmonic amplitudes for which the covariance matrix was computed. This procedure assumes the zonal wavenumber, but lets the data define dominant latitudinal structures of variations. These observed structures can then be compared with theoretical prototypes, the Hough function depictions of ψ.

Travelling waves would be manifest in two EOFs similar to the real and imaginary parts of a complex EOF analysis. They would be one-quarter of a spatial cycle (that is 90° of longitude

Table 2. Illustration of data used in the EOF analysis for a single zonal wavenumber s of stream function at 300 hPa. There are a cosine [A(t)] and sine [B(t)] coefficient defining the longitudinal location of the sinusoids and a value for meridional indices, $l - s$, defining the latitudinal structure. There are 12 variables describing each zonal wavenumber

Data are 29 220 observations of large scale spherical harmonics for each zonal wavenumber, $s = 1$, 2, 3 and 4						
$l - s$	0	1	2	3	4	5
Cos coef.	$A(t)_0$	$A(t)_1$	$A(t)_2$	$A(t)_3$	$A(t)_4$	$A(t)_5$
Sin coef.	$B(t)_0$	$B(t)_1$	$B(t)_2$	$B(t)_3$	$B(t)_4$	$B(t)_5$

for $s = 1$ and 45 for $s = 2$, etc.) out-of-phase and their Principal Components (PCs), or time series of amplitudes, would be one-quarter cycle out-of-phase in time. To compare propagation and periods with the expected westward propagation and the periods of Table 1, time series of PCs were computed by projection of the basic data onto the EOFs. Cross-spectra between the PC time series of 29 220 values of likely pairs of EOFs are examined for coherence at expected frequencies and for phase angles that are consistent with westward propagation.

4. Results

A summary of results is presented here. Complete results are posted at http://www.cgd.ucar.edu/cas/ram/rossbywaves.html, hereafter referred to as 'the Web Page'.

The analysis was carried out first using the basic data in order to establish, with minimum processing that might bias the results, the existence of disturbances in the Reanalyses similar to the theoretical prototypes. Then it was repeated with data that are bandpass (BP) filtered at the expected periods listed in Table 1. Lindzen et al. (1984) warned against effects of narrow BP filtering and we must be cautious when interpreting BP results here. In particular, filters used have tapered, but non-zero, weights that extend 41 (narrow BP) and 21 (less narrow BP) days before and after an event so that a disturbance isolated in time may appear to last longer than it actually does.

CEOFs (Wallace and Dickinson, 1972; Barnett, 1983; Horel, 1984) are well suited to isolated travelling disturbances in filtered data. Results of a CEOF analysis of the BP data are included in Section 4.2.3. Again the MATLAB EIG routine was used, this time on a 12 × 12 complex covariance matrix estimated from the 'complexified' data (von Storch and Zwiers, 1999, p. 359). The complexified time series is determined using the HILBERT transform routine of MATLAB.

4.1. Results—basic data

4.1.1. EOFs and horizontal structures. Columns of Table 3 contain the EOFs for the zonal wavenumber 1 ($s = 1$) analysis. Rows in Table 3 are EOF weightings for each meridional index, $l - s$. Weightings in the Table were normalized so that their sum of squares is equal to one and then multiplied by 100. Alternate rows are for the cosine (A) and sine (B) projections of a given meridional index ($l - s$). The bottom row has the percent variance explained by each EOF.

The Hough function depictions of Fig. 1 show that the MRG waves look very much like the $l - s = 0$ associated Legendre polynomial. As a result, it is easy to see from Table 3 that the likely EOF pair most reflecting the $s = 1$ MRG mode is EOF12 and EOF11. The number refers to the order of the EOF determined by the percent of variance that it explains with EOF1 explaining most and EOF12 explaining least. EOF12 and EOF11 project almost exclusively onto the $l - s = 0$ associated Legendre polynomial. Inspection of Fig. 3, which shows two-dimensional pictures resulting from the EOF weightings applied to the associated Legendre polynomials suggests that EOF12 and 11 are one-quarter cycle out-of-phase in space. In the same way, EOF8 and 7 are likely reflections of the 5-Day Wave, and EOF10 and 9 the 10-Day Wave. These three EOF pairs explain about 5 (2.1454 + 2.4323), 15 and 13% of the variance of the first six degrees of $s = 1$ waves, respectively.

After those EOFs it is more difficult to pick the appropriate EOF pairs probably because, as expected from theoretical treatments, the background winds distort the slower propagating

Table 3. Columns contain the EOFs for the $s = 1$ analysis. Rows in the Table are the weightings for each meridional index, $l - s$. Alternate rows represent the cosine [A(t)] and sine [B(t)] coefficients as indicated in the right-hand column. Values are normalized so that the sum of their squares is one and for the table, they have been multiplied by 100. The percent variances explained by each EOF, rounded to the nearest whole percent, are indicated in the bottom row

$l - s$	**12**	**11**	**10**	**9**	**8**	**7**	**6**	**5**	**4**	**3**	**2**	**1**	
0	−98	−18	−4	−2	−6	3	1	3	−1	−2	2	−1	**A**
0	−17	98	1	−10	−1	1	−5	5	0	4	4	1	**B**
1	−4	−1	−1	13	82	9	−19	19	34	10	4	−32	**A**
1	−3	2	−31	−6	20	−63	46	−2	25	19	5	39	**B**
2	0	7	−18	87	−13	1	14	19	−14	1	33	−4	**A**
2	5	−3	−80	−10	−22	22	−33	3	17	31	−9	−4	**B**
3	1	−2	2	−7	18	50	1	−32	11	1	54	56	**A**
3	0	−3	−17	−20	33	−5	2	5	−85	28	15	−5	**B**
4	4	−9	19	−25	−23	−27	−32	52	13	15	59	−3	**A**
4	−6	0	30	25	−6	−26	−40	−51	2	60	−5	2	**B**
5	1	0	3	−17	−16	17	55	−23	16	32	29	−59	**A**
5	0	−2	26	5	−4	35	26	49	3	54	−35	29	**B**
%var	2%	2%	6%	6%	7%	8%	8%	9%	11%	12%	14%	15%	

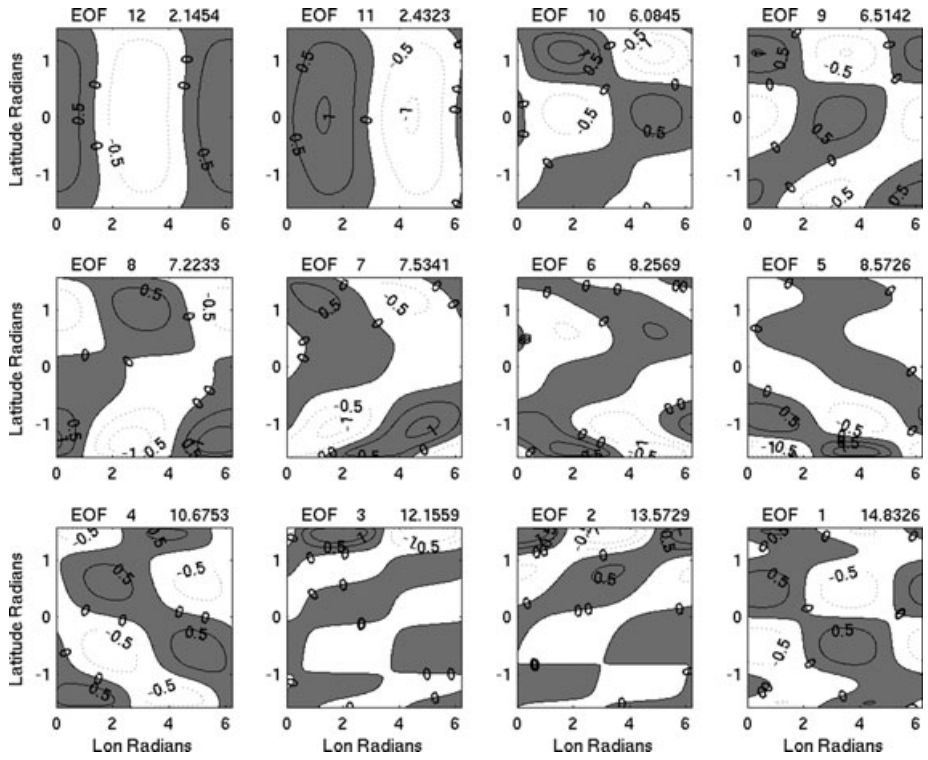

Fig. 3. EOFs of the basic ψ (stream function) data for zonal wavenumber 1 ($s = 1$). Each panel is a map going eastward from the Greenwich Meridian for 2π radians (horizontal) and from the South Pole ($-\pi/2$ radians) to to the North Pole ($+\pi/2$radians). Shaded values are positive. EOF weightings for these maps are shown in Table 3. Amplitudes are arbitrary. The EOF number and percent variance explained by each EOF are indicated above the upper left and upper right of each panel, respectively. EOF1 (lower right) explains the most variance and EOF12 (upper left) the least.

higher modes. Similar two-dimensional maps determined from EOFs for $s = 2$, 3 and 4 can be found on the Web Page. These maps will be referred to as EOFS although, strictly speaking, the EOF weightings apply to the amplitudes of the associated Legendre polynomials and not directly to a two-dimensional array of gridpoint values.

In an effort to make the selection of EOF pairs more objective, latitudinal profiles of the EOFs were taken from the longitude where the EOF was a maximum in a root mean square (RMS) sense. For example, the profile for EOF12 in Fig. 3 was taken from longitude 6.1 radians and that for EOF11 from longitude 1.4 radians. Root mean square differences (RMSD) between these EOF profiles and those of the Hough functions were then computed. In three cases the EOF pair selected from Fig. 3 to represent a given $s = 1$ wave mode was composed of the two EOFs with smallest RMSD with respect to the corresponding Hough function.

The other two cases were the pair chosen for the 5-Day Wave (EOF7 and EOF8), and that chosen for the 16-Day Wave (EOF4 and EOF2). The RMSD was smallest between EOF1 and the Hough ($s = 1$, $l = 2$), 5-Day Mode, with EOF7 and EOF8 following in that order. Cross-spectra to follow between PCs of EOF1 and EOF7 and those between EOF1 and EOF8 had sharp coherence maxima exceeding 0.5 at 5-d periods. PC8 led PC1 by a quarter of a cycle consistent with westward propagation. PC7 and PC1 are out-of-phase. Undoubtedly all three EOFs and PCs are reflecting the 5-Day Wave. We chose EOFs 7 and 8 to represent the 5-Day Wave because they explained about the same amount of variance (7% from Fig. 3), and, as we shall see, their PCs also suggest westward motion. In the case of the Hough (1,4), 16-Day Wave, EOF8 and EOF7 had smallest and nearly equal RMSD. It is shown in Fig. 5 to follow, that at a 16-d period, cross-spectrum between PC7 and PC8 suggest eastward propagation. As a result, EOF4 and EOF2 were selected for the 16-Day Wave because they are qualitatively similar to the Hough(1,4) mode (excepting the asymmetry of EOF2 evident in Figs. 3 and 4 to follow), and because cross-spectrum between their PCs is consistent with westward propagation.

This again emphasizes the difficulty in isolating the higher, or smaller latitudinal scale, modes. It is likely that their structures are dependent on changing background flow to an extent that they cannot be cleanly isolated by a single EOF pair. Actual asymmetries about the equator become large for theoretically predicted waves with large values of l. EOFs computed by season might show that asymmetries computed here are primarily reflecting larger amplitudes in the winter hemisphere as suggested by

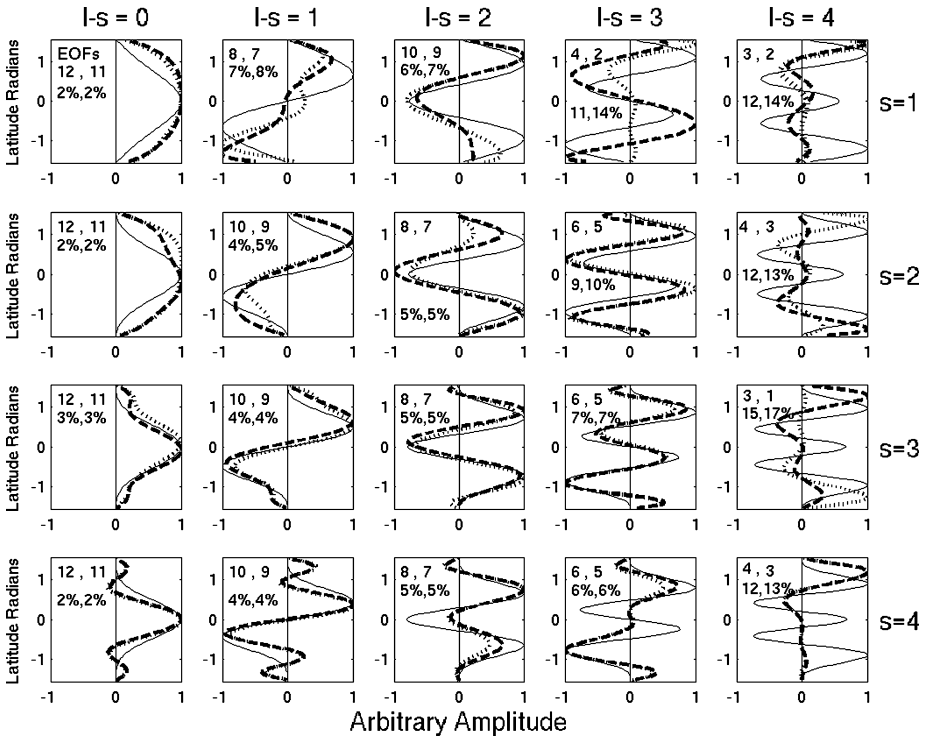

Fig. 4. Solid curved lines are the Hough function depictions of the latitudinal structure of ψ (stream function) for the $s, l-s$ mode in an atmosphere with an equivalent depth of 10 km like those of Fig. 1 (after Kasahara, 1976). Each row is for a different zonal wavenumber s, and each column is for a different meridional index, $l-s$. Selected EOF pairs and the percent variance that they explain are indicated in the upper left of each panel. Dashed line represents the first, or left-hand side, indicated EOF, and dotted line the second, or right-hand side indicated EOF. Profiles in the top row correspond to the EOFs shown in Fig. 3.

theoretical studies mentioned earlier. A further study of the possible roles played by more than two EOFs in depicting a wave mode and of the seasonal variations in these roles might shed light on evolving wave structures

To summarize the results, Fig. 4 compares the latitudinal structures of selected pairs of EOFs for all four wavenumbers to corresponding Hough functions for ψ. All EOF pairs in Fig. 4 have the smallest RMSD with respect to the indicated $s, l-s$ Hough mode except the two cases for $s = 1$ discussed above.

4.1.2. Cross-spectra and propagation. To assure that selected EOF pairs are coherent with one another, and that they reflect westward motion coherence squared and phase between their PC time series were computed by:

(1) Fourier transforming the PCs.

(2) Squaring coefficients to form periodograms.

(3) Multiplying the corresponding real and imaginary parts of the two transforms together.

(4) Computing a running averages of 584 periodogram values and of the cross-products to give smooth estimates of the spectra, $\mathbf{P_1}$ and $\mathbf{P_2}$, and the cospectrum, **C** and quadrature spectrum, **Q** (effective band width is 584/29220 cycles d^{-1}).

(5) Computing the squared coherence from $\mathbf{(C^2 + Q^2)/P_1P_2}$, and the phase from **Atan(Q/C).**

If, to first approximation, we assume that the data are independent this procedure results in spectral estimates with 1168 (2×584) degrees of freedom (*d.f.*). Assuming a null of zero, the resulting 95% significance level for the squared coherence is 0.0051 (Julian, 1975) and confidence limits for phase at a similar level depend also on coherence. For squared coherence = 0.1 it is about ± 0.17 radians (Jenkins and Watts, 1968, eq. 9.2.25). If we were to be conservative and assume 117*d.f.*, that is roughly 10 d between independent estimates, then the 95% significance level for the coherence squared is 0.051 and for phase ± 0.52 radians again assuming squared coherence = 0.1

Figure 5 shows the coherence and phase between the PC time series of pairs of EOFs for $s = 1$ of Figs. 3 and 4. In Fig. 5, statistically significant squared coherence (0.0051 for 1168*d.f.*) is practically indistinguishable from zero coherence. Vertical lines represent theoretical frequencies from Table 1. There is large coherence at 1.2 d periods of the MRG wave in the cross-spectrum between EOF12 and 11 PCs. The phase at 1.2 d (actually at nearly all periods) indicates that EOF11 leads EOF12 by about one quarter cycle, which from Fig. 3, confirms westward movement. The second coherence maximum near 5 d suggests that EOF11 and EOF12 project onto the 5-Day Wave as well. EOF7 and EOF8 look more like the expected 5-Day Wave and

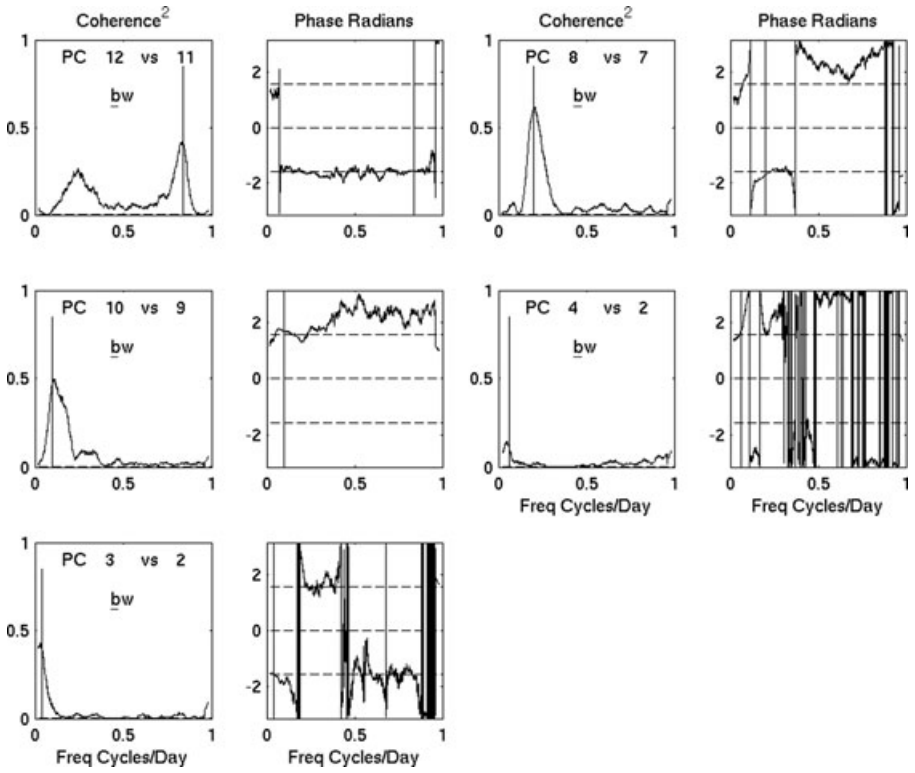

Fig. 5. Squared coherence (left of each pair of panels) and phase (right of each pair of panels) between the PC time series of selected pair of EOFs from Fig. 3 for $s = 1$. Phases are in radians and frequency in cycles d^{-1}. Negative phase angles means the first mentioned EOF (e.g. EOF12 in upper left panels) trails the second mentioned EOF (e.g. EOF11 in upper left panels). Vertical line in each panel marks the 1.2-, 5-, 10-, 18- and 28-d period predicted by Kasahara's (1980) analysis for $s = 1$. The 95% significance level assuming zero coherence and 1168*d.f.* of 0.0051 (dashed line) is barely distinguishable from the zero line. In the phase diagrams, $-\pi/2$, 0 and $+\pi$ are indicated by the horizontal dashed lines.

cross-spectrum of their PCs is consistent with 5-d periods and westward movement too. Same is true for the 10-Day Wave though in this case the PC of EOF10 leads that of EOF9, again consistent with westward propagation of EOF patterns shown in Fig. 3. Coherence maxima and westward movement is also confirmed at 16- and 25-d periods for PCs of EOF4 and 2 and those of EOF3 and 2, respectively.

Figures depicting parallel spectral results for the PCs of pairs of EOFs for $s = 2$, 03 and 4 can be found on the Web Page. Figure 6 is presented by way of summary. It shows the coherence squares for each selected EOF pair for all four zonal wavenumbers. Each pair has the smallest RMSD from the respective Hough function but for the two exceptions for $s = 1$ (5- and 16-Day Wave) discussed above. Where squared coherence have a maximum at the expected theoretical frequencies, phase angles are a quarter of a cycle and consistent with westward propagation (Fig. 5 for $s = 1$; see the Web Page for $s > 1$). Consistencies between the horizontal structures, coherence, and phase provide evidence for the existence of the wave mode $s = 1$ and 2, $l - s = 0$, 1, 2, 3 and 4 and for $s = 3$, $l - s = 0$, 1 and 2 (results for $l - s = 3$, 4 and 5 suggest eastward propagation).

For $s = 4$, $l - s = 0$ and 1, the EOF structures within 45° of the equator and their propagation are consistent with the MRG wave and the first symmetric mode. In addition, the relative maximum in coherence and phase that is consistent with westward propagation is between 6 and 7 d for the $l - s = 1$ mode, which is slightly larger than the prediction from Table 1 of 5.2 d.

It is interesting to note that the EOF pairs chosen for all four MRG waves appear to project onto the 5-Day Wave as well. The large squared coherence of some of the $l - s > 2$ modes that are not at the predicted frequencies are associated with eastward propagation. Also, the $s = 1$, 2, 3 and $l - s < 3$ waves are large enough so that spectra of their corresponding PCs have discernable peaks at predicted frequencies that differ from red noise.

4.2. *Results—filtered data*

Above results are based on data with relatively little filtering. The fact that coherence squares tend to maximize near the expected theoretical frequency is powerful evidence that an EOF pair reflects a free Rossby wave. To look further at the waves, data were also subjected to BP filtering. The filters were designed to isolate variations near the predicted periods of Table 1. Figure 7 shows the response of each BP filter. The analysis procedure described above was repeated, but this time for each

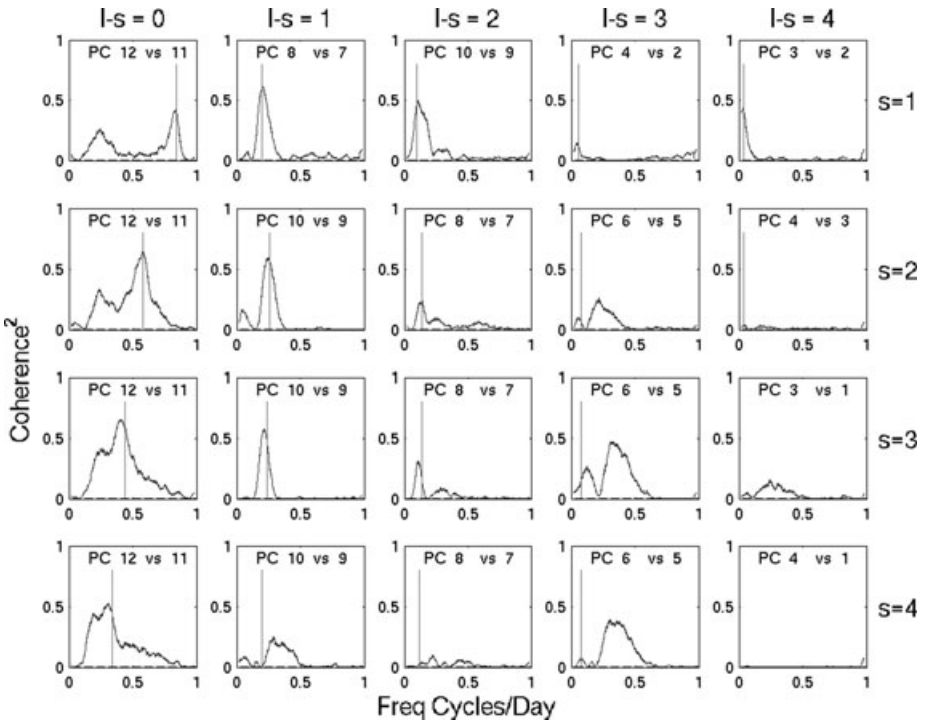

Fig. 6. Coherence squared between the PC time series of selected pairs of EOFs from Fig. 4. Each row is for a different zonal wavenumber, s and each column is for a different meridional index, $l - s$. Vertical line in each panel marks the predicted period for a given mode by Kasahara's (1980) analysis.

of the filtered data sets. Here we present the most relevant results but all can be seen on the Web Page.

4.2.1. EOFs and horizontal structures. The left hand two columns of Fig. 8a–c present the leading two EOFs of the filtered data for $s = 1$, 2 and 3 respectively. By 'leading' is meant the EOFs that explain most of the variance. The right hand column contains the central period of the filter taken from Table 1 and the percent variance of the filtered data explained by the two EOFs We have seen in Fig. 3 and Table 3 that the two EOFs corresponding to the 1.2-Day MRG wave explain just under 5% of the variance of the basic data, and that they are EOF11 and EOF12, meaning they explain the least variance of all the EOFs. Nearly identical EOFs shown in Fig. 8a explain 37 and 36% of the variance in the 1.2-d, bandpass, filtered data, and they are the leading EOFs for this limited frequency band.

Figure 8d shows results, not for the leading $s = 4$ EOFs of the 2.9 and 5.2-d filtered data, but for the runnerups, EOF3 and EOF4. Since they are not the leading EOFs, they don not explain most of the variance in their respective frequency band; however they have the smallest RMSD from the $s = 4$, $l - s = 0$ and 1, waves, and, as it turns out, they are the only EOF pairs of the $s = 4$ data that are consistent with westward propagation.

Most of the EOFs in Fig. 8 have the smallest RMSD with respect to their corresponding Hough function depiction of ψ with the exceptions of $s = 1$ and 2, $l - s > 3$.

4.2.2. Cross-spectra and propagation. Columns 3 and 4 of Fig. 8 show the squared coherence and phase between PCs of the corresponding EOF pairs based on the filtered data. High coherence away from the frequencies of the relatively narrow bandpass filters arise because of tiny side lobes (see Fig. 7), and therefore result from ratios of very small numbers.

With filtered data, frequencies are specified, but coherence between PCs need not be high. The coherences between the PCs of the EOF pairs shown in Fig. 8 are significantly different from zero at the filtered frequencies, and phase relations indicate a westward propagation. Taking the MRG wave ($l - s = 0$), for example, for $s = 1$ PC2 leads PC1 by a quarter of a cycle at 0.82 cycles d^{-1} (Fig. 8a), while for $s = 2$ and 3 PC2 leads PC1 by a quarter of a cycle at 0.58 (Fig. 8b) and 0.43 cycles d^{-1} (Fig. 8c), respectively. For $s = 4$ PC3 leads PC4 by a quarter cycle at 34 cycles d^{-1}.

It should be noted that for larger values of l maxima in the squared coherence tend to be at slightly lower frequencies than that of the theoretical predictions of Table 1.

4.2.3. CEOF analysis of filtered data. CEOFs were estimated for each of the filtered time series to round out the data analysis. To summarize, we adapt Barnett's (1983) notation and write

$$U_n(k) = A_n\, B_n^*(k),$$

where $B_n^*(\boldsymbol{k})$ is the complex conjugate of the nth CEOF, A_n is its complex amplitude (PC), and $U_n(\boldsymbol{k})$ is, then, the nth CEOF's

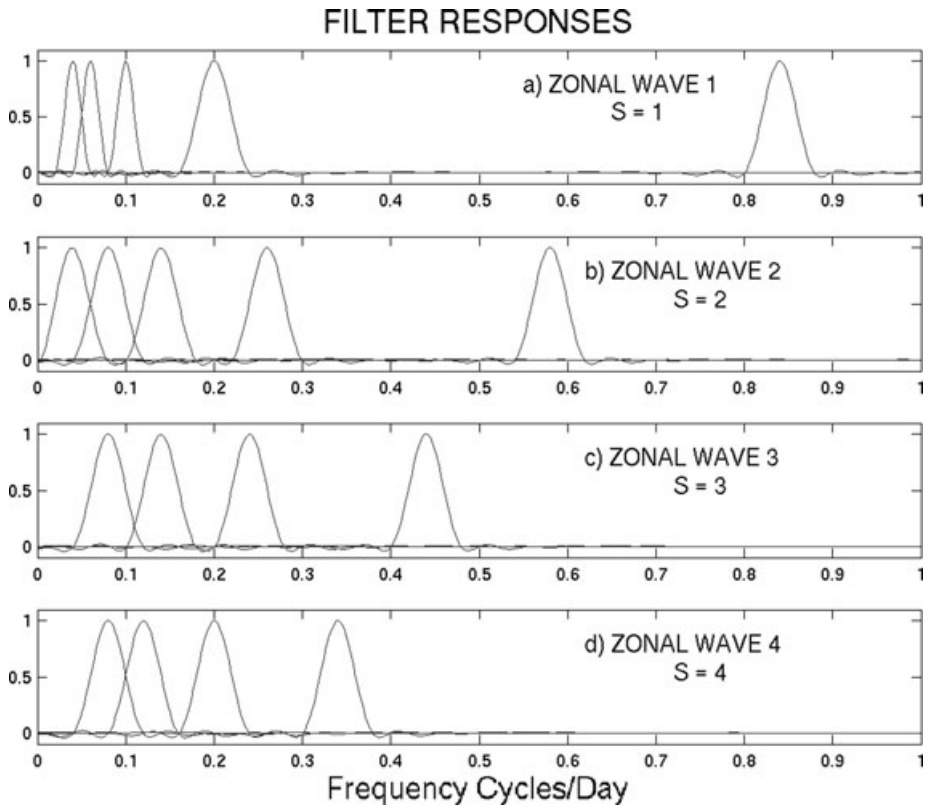

Fig. 7. Bandpass filter responses of filters used on $s = 1$, 2, 3 and 4 (top to bottom) data. Bandpass width is 0.04 cycles d^{-1} at a response of 0.5 for most of filters. This filter has the equivalent of 87 weights spanning 43 d. A narrower bandpass (0.02 cycles d^{-1}) was used for $s = 1$ data at 9.91, 18.39 and 28.08 d to reduce overlap. It has the 167 weights spanning 83 d. Note that there are small side lobes which allow tiny amplitude variations at nearly all frequencies.

contribution to the amplitude of the kth (s, l) associated Legendre polynomial. The real part of $U_n(k)$ was used to construct two-dimensional maps as in Fig. 3, after taking an arbitrary value for A_n. These maps for all CEOFs can be found on the web page. Figure 9 shows latitudinal profiles determined from the maps for the wave modes identified in the previous sections.

Most profiles in Fig. 9 are for the leading CEOF of a given filtered data set. Those that are not ($s = 4$ modes) are for the CEOFs that resulted in the smallest MSD from the Hough function depiction of ψ of the relevant wave. In all cases the single CEOF chosen explains nearly as much variance as the combined total of the EOF pairs of Fig. 8. Not surprisingly, comparison of Figs. 4 and 9 reveal strong similarities between the EOFs and the CEOFs.

5. Summary of observations

Both the basic and the filtered data give evidence for wave modes as indicated in Table 4. A 'YES' in the Table signifies our conclusion that there is sufficient evidence for the existence of a mode. A 'NO' in the Table does not prove a mode never exists as a discrete wave, but only that our method which averages over all seasons and 40 yr, does not provide sufficient evidence that they do. In addition, some subjectivity is unavoidable in assessing evidence for the higher order and degree, or slower moving, modes. It is safe to say that modes with $l < 4$ are easily identified which is a conclusion consistent with the predictions of Kasahara (1980), Salby (1981a,b) and Branstator and Held (1995).

5.1. Earlier published observations

Because the Reanalysis data are dependent on a model, one might argue that the above results simply reflect the model influence and not necessarily reality. However, evidence for the existence of large-scale, free Rossby waves goes back at least 50 yrs (e.g. Kubota and Iida, 1954). In the intervening time, studies reporting similar results have been based on many data sources and analysis methods. Since early observational works have already been reviewed, we limit the following to papers written after 1980 that deal with several modes.

Ahlquist (1982, 1985) investigated about three yr (1976–1979) of National Meteorological Center (NMC) operational analyses. The data consisted of u, v and Z at various levels including 1000, 850, 500 and 200 hPa. They were fit to the Lamb

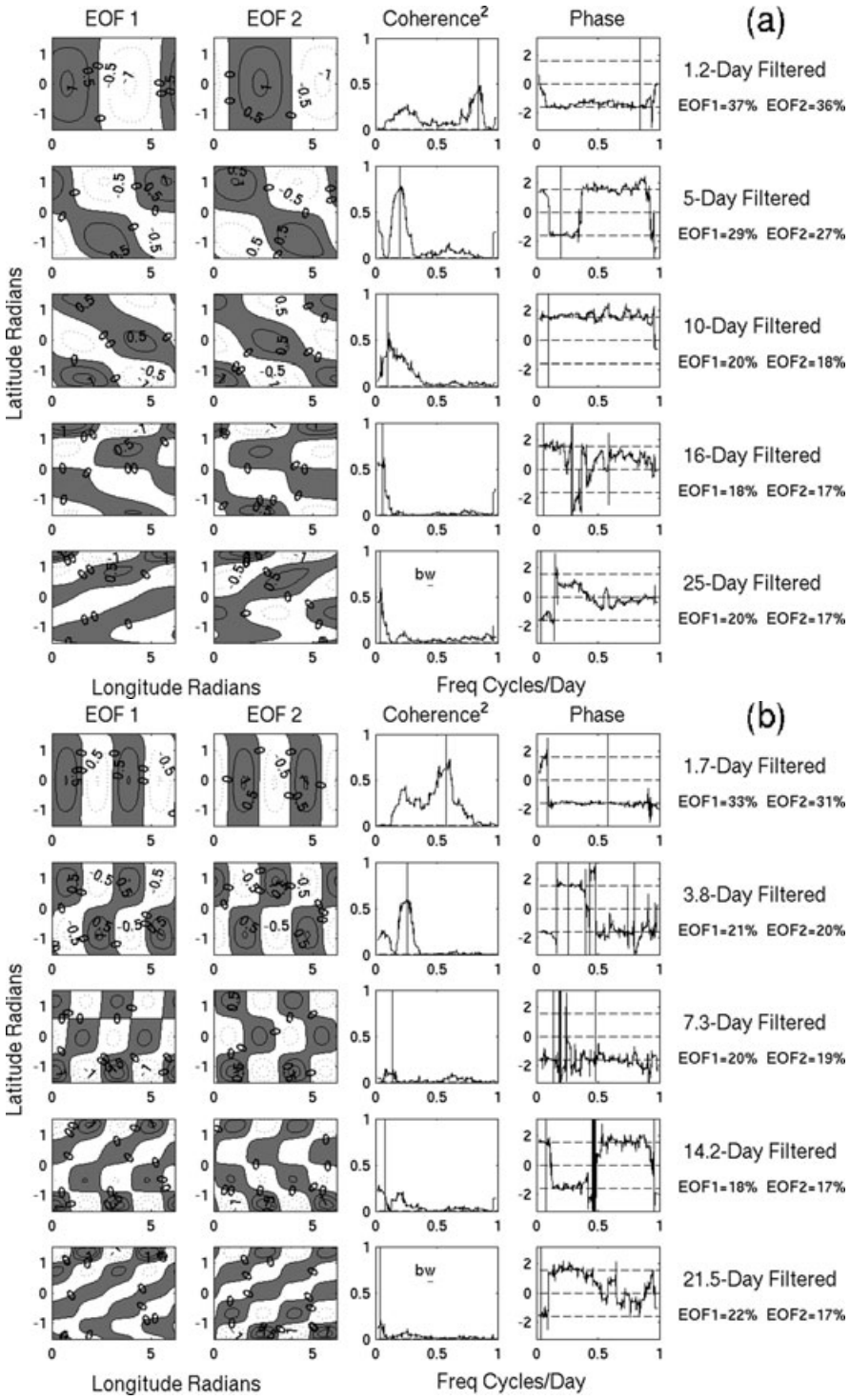

Fig. 8. EOFs (left-hand side two columns), squared coherences (middle column), and phases (fourth column) between PCs from data filtered at indicated periods (right-hand side column). Vertical lines in the coherence and phase panels also mark the predicted period for a given mode by Kasahara's (1980) analysis. Large squared coherence away from these periods result from sidelobes of the filters and therefore from the ratios of very small numbers. EOFs are leading ones for the filtered data of s 1 (a), $s = 2$ (b) and $s = 3$ (c). Percent variance of the filtered data explained is also included in the right-hand column. For $s = 4$ (d), results are for EOF3 and EOF4. Thick vertical line in the lower panel indicates relative coherence maximum likely to be related to the $s = 4, l - s = 1$ mode. The leading EOFs for $s = 4$ filtered data propagate eastward. Only results consistent with westward propagation are shown in Fig. 8. The 95% significance level assuming zero coherence and 1168*d.f.* of 0.0051 (dashed line) is barely distinguishable from the zero line. In the phase diagrams, $-\pi/2$, 0, and $+\pi/2$ are indicated by the horizontal dashed lines.

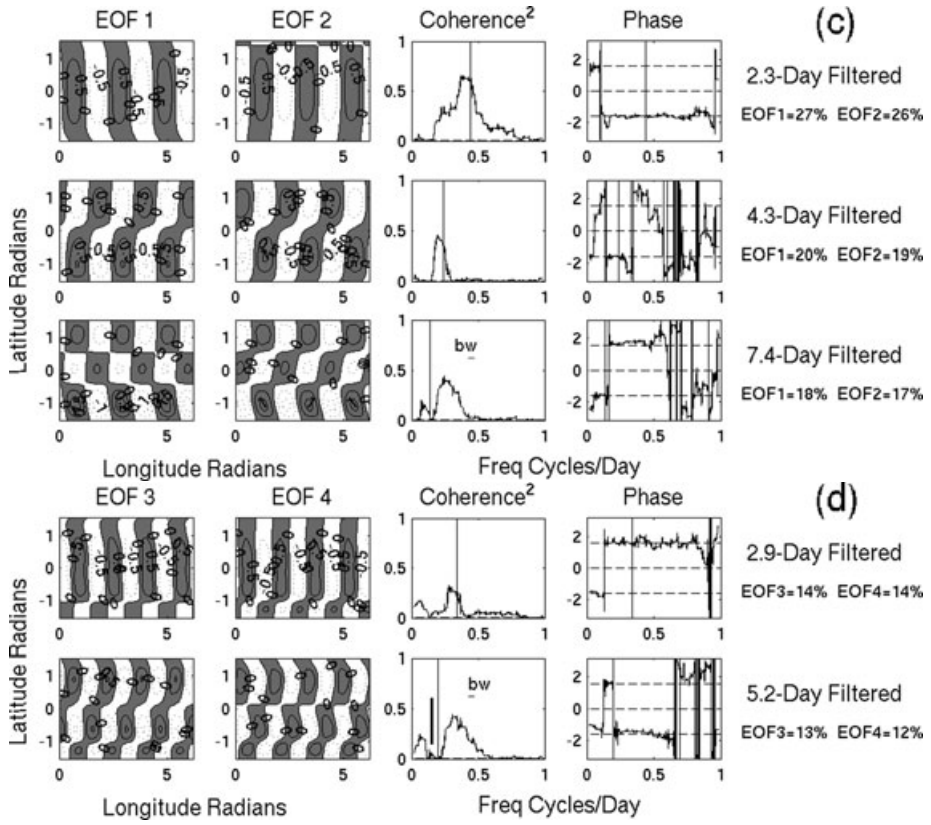

Fig. 8. cont'd

mode vertical structure and Hough function horizontal structures. Spectra showed extra variance at frequencies expected by theory for 14 modes. Thirteen of these are indicated in Table 5 by 'A82'. The fourteenth is the $s = 2, l = 6$ mode which is outside the range of the Table.

Lindzen et al.'s (1984) study was based on European Center for Medium Range Forecasts (ECMWF) analyses of 00 UTC and 12 UTC data from the First Garp Global Experiment (FGGE) of 1979. They considered the first three meridional modes, excluding the MRG waves, associated with $s = 1$, 2 and 3. They projected 500 hPa data onto Hough functions, Fourier transformed the coefficients in time, and filtered out the eastward propagating components. The remaining westward propagating components provided evidence for all nine wave modes (indicated in Table 5 by 'L84'). They emphasized the time variations of the waves and their episodic nature. Lindzen et al. also looked at FGGE analyses made by Goddard Laboratory for Atmospheric Sciences (GLAS), and found that their was good agreement between amplitudes and phases for seven out of the nine modes to show results were not an artefact of one of the analysis methods.

Venne (1989) made no a priori assumptions about the latitudinal structure of wave modes he investigated. He computed CEOFs of NMC data from 18 levels between 850 and 2 hPa and from latitudes between 85N and 85S. The data were from four northern winters between 1978 and early 1982. Each 'winter' consisted of 120 d starting between 9 September and 1 November depending on data availability. Before the EOF analyses, data were BP filtered at frequencies suggested by Kasahara (1980), Salby (1981b) and some earlier observations. Venne finds evidence for 12 modes. Eleven are indicated in Table 5 by 'V89'. The twelfth is the $s = 5, l = 6$ mode which is not included in the Table.

Hirooka and Hirota (1989) examined $s = 1$ and 2 modes in six and one-half years of data from 850 to 1 hPa. Like Venne, they too made no a priori assumptions about the latitudinal structures. They attempted to isolate wave modes from the westward propagating part of space–time spectra at theoretically predicted frequencies. They were able to identify several modes at 1 hPa which are indicated in Table 5 by 'H89'. They constructed a 'calendar' of the appearance various modes and showed, like Lindzen et al. (1984), their episodic nature. In addition, they documented frequent (primarily in solstice conditions) confinement of the smaller scale modes to the winter hemisphere.

Four years (1984–1987) of ECMWF operational analyses were studied by Elbern and Speth (1993). Data from 13 levels between 1000 and 30 hPa from 00 UTC each d were included. Like Ahlquist, Elbern and Speth projected their data onto the theoretically predicted vertical and horizontal structures of various wave modes and looked at their spectra for extra variance at predicted, westward frequencies. Their positive results are

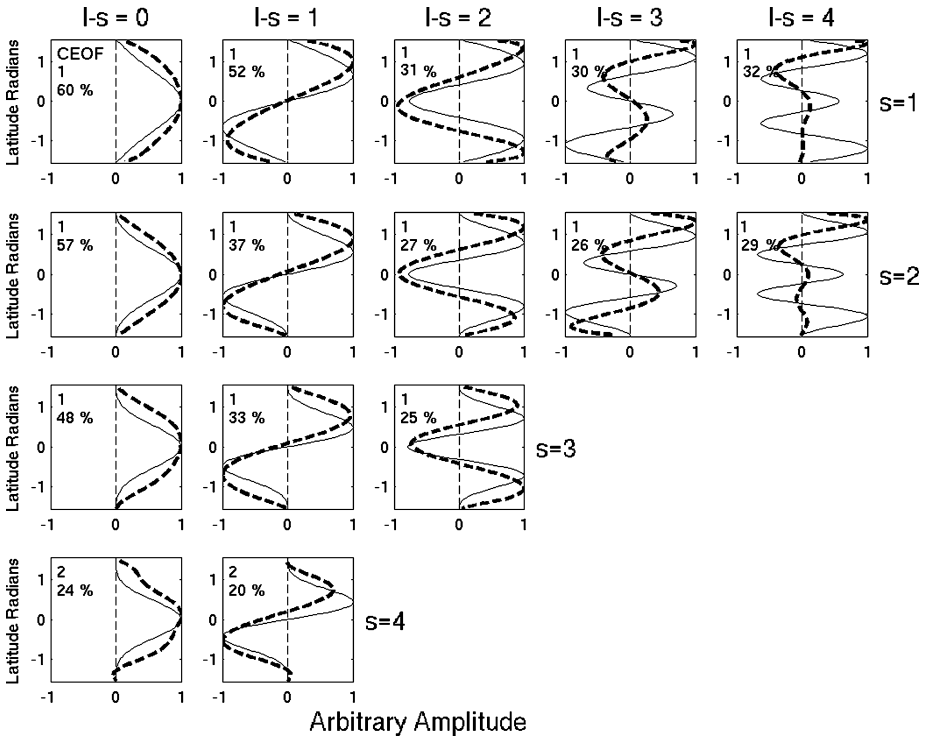

Fig. 9. Solid curved lines are the Hough function depictions of the latitudinal structure of ψ (stream function) for the $s, l-s$ mode in an atmosphere with an equivalent depth of 10 km like those of Fig. 1 (after Kasahara, 1976). Each row is for a different zonal wavenumber s, and each column is for a different meridional index, $l-s$. Dashed lines are the latitudinal profiles determined from selected CEOFs. The CEOF number is indicated in the upper left of each panel with the number 1 meaning the CEOF that explains most of the variance. The percent variance explained by a CEOF is printed just below the CEOF number.

Table 4. Summary of the evidence for free Rossby waves in the NCEP/NCAR Reanalysis. Each row is for a different zonal wavenumber, s, and each column is for a different meridional index, $l-s$. 'YES' indicates evidence was reasonably clear in the basic data as discussed in Section 4.1 and in filtered data which is discussed in Section 4.2. No clear evidence was found in either data set for the modes marked with 'NO' and modes marked 'XXX' are those for which Kasahara's (1980) analysis provides no theoretical basis for their existence

	$l-s=0$	$l-s=1$	$l-s=2$	$l-s=3$	$l-s=4$
$s=1$	YES	YES	YES	YES	YES
$s=2$	YES	YES	YES	YES	YES
$s=3$	YES	YES	YES	NO	XXX
$s=4$	YES	YES	NO	NO	XXX

indicated in Table 5 by 'E93'. They judged evidence for a mode to be 'highly significant', 'significant' or 'moderate', a distinction which is not signified in Table 5.

Weber and Madden (1993) worked with 10 yr (December 1978–December 1988) of two-per-day, operational ECMWF analyses from seven levels between 1000 and 100 hPa. Most of their analysis was made on the 500 hPa level data. These data

Table 5. Summary of wave modes reported in the literature during the last 25 yr. Rows are for zonal waves one ($s=1$, top row) through zonal wave four ($s=4$, bottom row). Columns are for different meridional indices from $l=s$ (left-hand side) to $l=s+4$ (right-hand side). A82 (Ahlquist, 1982), L84 (Lindzen et al., 1984), V89 (Venne, 1989), H89 (Hirooka and Hirota, 1989), W93 (Weber and Madden, 1993), E93 (Elbern and Speth, 1993) and M (current analysis) are indicated

	$l-s=0$	$l-s=1$	$l-s=2$	$l-s=3$	$l-s=4$
$s=1$	W93 M	A82 L84 V89 H89 W93 E93 M	A82 L84 V89 H89 W93 E93 M	A82 L84 V89 H89 W93 E93 M	V89 H89 W93 E93 M
$s=2$	W93 M	A82 L84 V89 H89 W93 E93 M	A82 L84 V89 H89 W93 E93 M	A82 L84 V89 H89 W93 E93 M	A82 H89 E93 M
$s=3$	A82 W93 E93 M	A82 L84 V89 W93 E93 M	A82 L84 V89 W93 E93 M	L84 V89 W93 E93	XXX
$s=4$	A82 W93 E93 M	A82 V89 W93 E93 M	A82 W93 E93	XXX	E93

were projected onto Hough functions, the Hough function amplitudes were divided into seasons (December–January–Febuary, etc), and then subjected to space–time spectrum analysis. Modes which had spectral peaks at the westward frequency expected for the mode were judged to be present. In Table 5 a 'W93' indicates that the mode was judged to be present in at least one season. It is worthwhile noting that the two-per-day sampling used is needed to resolve the fast moving MRG waves of $s = 1$ and 2.

There is an extensive record of papers presenting evidence of free Rossby waves in the upper atmosphere. For example, Hirooka (2000) found evidence for the 5- and 10-Day Waves in near-global data from the Upper Atmosphere Research Satellite all the way to the mesopause (about 0 km). Forbes et al. (1995) looked at data from single stations and found evidence for the 16-Day Wave, and possibly for the 5- and 10-Day Waves, as high as 95 km. Their modelling suggested that the 16-d feature was consistent with the upward penetration of the tropospheric and stratospheric wave observed at the same time, the January, 1979 '16-Day Wave' (e.g. Madden and Labitzke, 1981; Smith, 1985).

It is clear that a variety of analysis methods applied to a variety of data sets provides evidence for the existence of several of large-scale, theoretically predicted free Rossby waves.

Finally, 'M' in Table 5 refers to results from NCEP/NCAR Reanalysis data already summarized in Table 4.

5.2. Wave amplitudes

Estimates of the average amplitudes of these waves range from several tenths of 1–2 hPa at the surface (Ahlquist, 1982) and 10–29 geopotential metres (gpm) at 500 hPa (Ahlquist, 1985). These 500 hPa amplitudes are at 40 N and not necessarily at the latitude of maximum amplitude. Madden's (1978) compositing of December–Febuary data suggested 5 and 60 gpm amplitudes of the $s = 1$, $l = 2$ (5-Day) and $l = 4$ (16-Day) modes. A look at relative amplitudes can be made by multiplying the percent variance explained by the EOF pairs of Fig. 4 by the coherence squares of Fig. 6. This gives a first order estimate of the percent of the 300 hPa, s and $l - s$ waves stream function variance explained by the free Rossby waves. These values are tabulated in Table 6. In view of the attention paid to the 16-Day Wave over the years, its relatively small value in Table 6 (2%) probably points to the fact the values in the Table are only crude estimates.

Table 6. Approximate percent of the variance of the basic data explained by a free Rossby mode. Each row is for a different zonal wavenumber, s, and each column is for a different meridional index, $l - s$

	$l-s=0$	$l-s=1$	$l-s=2$	$l-s=3$	$l-s=4$
$s=1$	2%	9%	6%	2%	10%
$s=2$	3%	5%	2%	2%	3%
$s=3$	4%	5%	3%	XXX	XXX
$s=4$	2%	<1%	XXX	XXX	XXX

Lindzen et al. (1984) showed that the presence of modes was episodic and, for example, the amplitude of the 16-Day Mode can range from zero to 70 or more gpm at 500 hPa in a matter of a few days. Madden and Labitzke (1981) described a particularly large disturbance of January 1979 that they suggested was the 16-Day Mode with an amplitude well over 100 gpm at 500 hPa and 60 N. Because this particular disturbance was confined to the Northern Hemisphere (Smith, 1985), its identification as a Rossby normal mode has been debated (Daley and Williamson, 1985); nevertheless, it is safe to conclude that, though variable, free Rossby waves can occasionally be large enough to be an important part of the large-scale circulation. Indeed, Lindzen (1986) showed that even on days when no single mode has a large amplitude their sum can still be as large as 70 gpm.

5.3. Seasonal variations.

Apparently there is not a large variation in wave activity with season. Ahlquist (1985) found a small seasonal variation in the 3 yr data that he examined. Six of the modes showed maximum amplitudes in December–Febuary. Lindzen et al. (1984) did not discern a seasonal variation in their data from 1979. Based on their 10-yr data set, Weber and Madden (1993) reported only a slight tendency for modes to occur more frequently in December–May and that they tended to have largest amplitudes in the December–Febuary period.

Figure 10 is presented to elucidate seasonal variations of the PCs selected here to identify free Rossby modes in the 40-yr NCEP/NCAR Reanalysis. The variable plotted is the quadrature contribution to the coherence ($\mathrm{Coh_q}$) between PCs of the EOF pairs of Fig. 8. Defining the two PCs for the jth d of the ith yr as $PC_a(i,j)$ and $PC_b(i,j)$, and $PC_b{}^{\mathrm{H}}(i,j)$ the Hilbert transform of $PC_b(i,j)$, then

$$\mathrm{Coh}_q(j) = \left\{PC_a(i,j) \times PC_b^{\mathrm{H}}(i,j)\right\}^2 \Big/ \left(\left\{PC_a(i,j)^2\right\} \times \left\{PC_b(i,j)^2\right\}\right). \quad (2)$$

The brackets are meant to represent the average over all years for the jth day of the year. The Hilbert transform shifts a time series by one quarter of a cycle at each frequency so $\mathrm{Coh_q}(j)$ can be thought of as the quadrature contribution to the squared coherence for the jth day. Hilbert transforms were computed by the HILBERT function in MATLAB.

The numbers in the upper right of each panel in Fig. 10 are the value of quadrature contribution to the squared coherence with the variables of (2) averaged over all yr and all d. Because PCs of the selected EOF pairs tend to be 0.25 cycle out-of-phase $\mathbf{C^2} \ll \mathbf{Q^2}$. As a result these quadrature contributions averaged over all years and all days can be compared directly to the squared coherences of Fig. 8. Differences result from the fact that the frequency averaging in Fig. 8 is a simple running average with

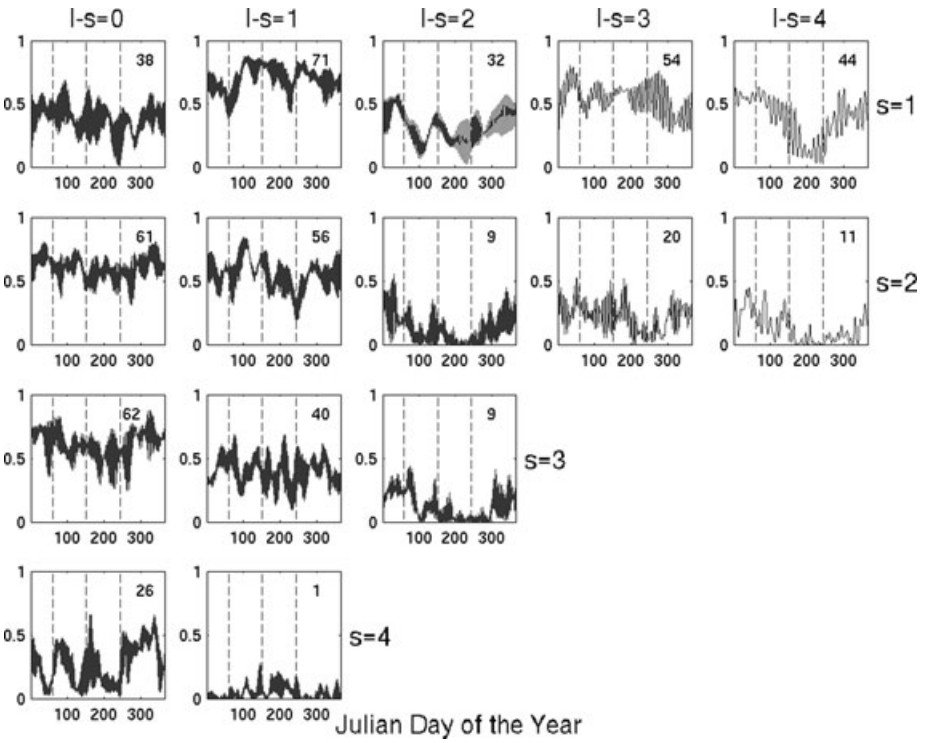

Fig. 10. The quadrature contribution to the squared coherence from (2) for PCs of the leading two EOFs (except for $s = 4$ case; see text) based on the filtered data averaged across the 40-yr record for each day of the year. Numbers in the upper right of each panel are the values given when the right-hand side of (2) is averaged over all years and all days. They have been multiplied by 100 for plotting purposes and they can be compared directly to the squared coherences of Fig. 8. Each row is for a different zonal wavenumber, s, and each column is for a different meridional index, l. Vertical dashed lines are at 1 March, 1 June and 1 September. Evident, fast variations have a frequency roughly half of the central frequency of the filters of Fig. 7 that result from the squaring process.

frequency width of 0.02 cycles d^{-1} (584/29220) as compared to the tapered filters of Fig. 7 whose widths are 0.04 or 0.02 cycles d^{-1} at their half power points.

The estimates of wave activity presented in Fig. 10 suggest a maxima in the northern winter half of the year for some of the smaller scale waves, and in that way they are consistent with earlier reports. It should be mentioned that the MRG wave of zonal wavenumber 3 ($s = 3, l - s = 0$) may show a slight tendency for maximum coherence in the northern winter half year. Upper atmospheric evidence for this, the 2-Day Wave, usually points to maximum activity in the summer hemisphere shortly after the solstice (see Vincent, 1984).

6. Effects of free Rossby waves on weather and circulation

The first work to directly relate weather to free Rossby waves was that of Burpee (1976). He showed that the percent of days with precipitation and thunder between about 15 S and 15 N from central Africa to the western Caribbean were modulated 5–10% by a global-scale 4–5 day pressure wave. Presumably the wave is the 5-Day Wave. Burpee pointed out that this modulation occurred in spite of the fact that surface divergence variations computed on the scale of the wave were small, on the order of 5×10^{-8} s^{-1}. Highest percent of days with precipitation and thunder were reported when the local 5-d pressure variation was a minimum. We are not aware of more published work relating precipitation directly to free Rossby waves which probably attests to the smallness and variability of the signal.

Free Rossby waves have also been tentatively linked to blocking episodes. Lindzen (1986) pointed out that a blocking episode is often defined by persistence in variables on the order of several days. Some of the slower free modes have local timescales on this order so that persistence so defined might simply reflect a slow moving free wave. Quiroz (1987), Lejenäs and Döös (1987) and Lejenäs and Madden (1992) have all documented the frequent coincidence between westward travelling waves and blocking episodes. These studies are suggestive of a role for free Rossby waves, but their importance for blocking needs further definition.

In isolation, free Rossby waves transport neither momentum nor heat. Nevertheless, the interference between them and forced, stationary waves can produce time variations in the transports. Palmer (1981), Lindzen et al. (1982), Salby (1984) and Salby and Garcia (1987a) among others explain how this can come about. The interference between stationary and travelling waves was shown to produce variations in heat and momentum transports

in models (Hirota, 1971; Clark, 1972; Geisler, 1974; Garcia and Giesler, 1981; Lindzen et al., 1982) and in observations (Madden, 1975, 1983; Hirooka, 1986). This interference phenomenon is, by itself, a linear one that leaves no lasting change. However, with large amplitudes it can give way to more dramatic, non-linear processes like wave breaking (McIntyre and Palmer, 1983) that are irreversible.

Large-scale atmospheric pressure variations can affect the Earth and oceans. Eubanks et al. (1988) related observed motions of the Earth's pole to the 16-Day Wave. In a somewhat related study, Lejenäs and Madden (2000) estimated the size of changing mountain torques resulting from the passage of free Rossby waves of typical amplitudes. They found changes exceeding 2 Hadleys (1 Hadley $= 10^{18}$ kg m^{2}s^{-1}) which are small relative to other subseasonal variations that can exceed 40 Hadleys (Madden and Speth, 1995), but with earth orientation data becoming more accurate they should be large enough to be detected.

Ponte (1997) has performed numerical experiments with a shallow water model to illustrate expected responses of the ocean to forcing by the 5-Day Wave. These responses too, along with possible others due to other free modes, may be detectable. Related data provide a fertile subject matter for observationalists.

7. Free Rossby waves in models

7.1. General circulation models (GCMs)

The most important papers dealing with free Rossby waves in a GCM are those Salby (1981a,b). His results are often used to help interpret observations of the real atmosphere. They provide a framework from which one can better anticipate the effects of realistic background winds and temperatures on the simple wave structures of free modes of the Tidal Equations. He used a constant vertical velocity from pole to pole for symmetric modes and constant amplitude but with a change of sign at the equator for antisymetric modes to force the model, and changed its frequency until the response reached a relative maxima. The maxima mode responses occurred near expected frequencies in the lowest two scale heights, excited wave structures were nearly unchanged from those in an isothermal, resting atmosphere. This was true for $s = 1$, 2 and 3 and $l = s, s + 1, s + 2$ and $s + 3$ modes. For larger l values, maximum response was less sharply tuned to a single frequency. His conclusion was that at least modes with $l < 4$ should be identifiable in data from the real atmosphere.

Salby's GCM experiment was designed to study free waves. There have been relatively few diagnoses for the presence of free Rossby waves in general GCM simulations originally run for other purposes. The earliest were those of Hayashi (1974) and Tsay (1974). Hayashi found the $s = 1, l = 2$ (5-Day) wave in a run of the Geophysical Fluid Dynamics Laboratory (GFDL) grid point GCM of the time. Similarly, Tsay described the 5-Day Wave in the National Center for Atmospheric Research GCM. In a paper to introduce the method of maximum entropy spectrum analysis, Hayashi (1981) found evidence for the 5- and 16-Day Waves in a nine level, 30 wave, spectral GFDL GCM. He and Golder (1983) compared results from model runs (GFDL, nine level, 15 wave spectral model) with and without mountains and found the 5- and 16-Day Waves in both.

Later, the 5-, 16-Day, the $s = 2, l = 3$ or 4-Day (Hirota and Hirooka, 1984), and the $s = 3, l = 3$ 2-Day (MRG) Waves were found in the GFDL SKYHI model by Manzini and Hamilton (1993). The SKYHI model is a comprehensive GCM including the troposphere, stratosphere and mesosphere.

Hamilton (1987) also computed the space–time spectra of output from the Canadian Climate Centre GCM and found that the 5-Day Wave was present. In addition, he found evidence for the 4-Day Wave. Evidence for the 16-Day Wave was not clear, and during some periods of westward propagating variance of about the right timescale the wave was distorted with much larger amplitude in the winter hemisphere

7.2. Forecast models

In the second issue of *Tellus*, Charney and Eliassen (1949) reported on a discrepancy in the earliest numerical forecast with a barotropic model that they argued was caused by an unrealistically large free, travelling wave and small forced, stationary one. They showed that mountain and frictional forcing improved the stationary perturbation and, in turn, the forecast.

Improving the model's forcing of stationary perturbations as attempted by Charney and Eliassen gets at the root of the problem of properly proportioning the energy of the initial conditions between free and forced waves. This was beyond the capability of early forecast models so empirical methods were used to 'control' the large-scale waves. For example, Wolff (1958) simply held zonal waves one, two and three fixed and Cressman (1958) and others, in an effort '. . .to include in the forecast models proper descriptions of the physical processes which actually occur in the atmosphere, wherever possible . . .', introduced an empirically determined amount of divergence into the forecast equations. These adjustments improved the forecasts but not the forcing of stationary waves.

Lambert and Merilees (1978) returned to the problem of forecasting the large-scale waves from the viewpoint of the superposition of free and forced waves as framed by Charney and Eliassen. They examined 15, 96-h forecasts of a hemispheric, spectral model and found erroneously large amplitude $s = 1$, $l - s = 1$ and $s = 2$, $l - s = 2$, waves propagating westward at speeds consistent with Kasahara's predictions (Table 1). They concluded that because of a failure to simulate the quasi-stationary forced waves correctly, initial conditions presented to the model were improperly partitioned between quasi-stationary and transient components. In a similar way, Daley et al. (1981) found that spurious excitation of large-scale free Rossby waves contributed to errors in their forecast experiments.

Hollingsworth et al. (1980) showed that the error fields of ECMWF forecasts were dominated by the long waves, a result unexpected by predictability theory (Lorenz, 1969). They found that when the behaviour of a large-scale wave mode could be regarded as the sum of a stationary part and a transient part in the model, then the largest errors were in the stationary part. Forcing of the stationary waves in models has improved since then with better mountain forcing (e.g. Wallace et al., 1983), better understanding of tropical forcing (e.g. Heckley and Gill, 1984), and the like to a point at which Ferranti et al. (2002) estimate that the amplitude of systematic, or the model climate errors have been reduced by a factor of eight since the early 1980s. This better forcing of the stationary waves undoubtedly has improved the partitioning of the initial energy between stationary and transient waves.

8. Exciting free Rossby waves

Even free waves need some kind of excitation in order to exist in the face of dissipation by radiation and friction. Garcia and Geisler (1981) demonstrated one possible forcing mechanism in a relatively simple quasi-geostrophic β-plane channel model. Zonal winds were prescribed to vary with a realistic red noise spectrum over topography. The resulting red noise vertical motions excited one external and two internal normal modes of the model. This suggested that random forcing in time and space would preferentially excite the real atmosphere's free waves. Salby and Garcia (1987b) and Garcia and Salby (1987) expanded on the idea of random forcing exciting free Rossby waves in their study of the response of the primitive equations of a spherical baroclinic atmosphere. In their case, the forcing was episodic heating designed to mimic observed convective heating in the Tropics.

Exact roles of mountain forcing and convective heating in exciting free Rossby waves are not fully understood. Probably, just as in the forcing of the stationary waves, both forces play important roles. Manzini and Hamilton (1993) forced a linear model with heating of a SKYHI model simulation and found that free waves were not excited. Since the free waves were evident in the SKYHI simulation, they concluded that the heating was not a major source for the excitation. Cheong and Kimura (1997, 2001) compared the horizontal structures of waves found in a numerical simulation with observed 5-, 10- and 16-Day Waves. They argued, primarily because of NW-SE tilt in the observed and simulated waves, that the interaction between time varying zonal winds and the topography of Antarctica was important in exciting the waves.

Hayashi and Golder (1983) showed in their study of model runs with and without mountains, that the free wave amplitudes were only slightly reduced in the no mountain case. This suggests that mountain forcing is not the only phenomenon that can excite the waves. On the observational side, Hamilton (1985) found that the variance in sea level pressure associated with the 5-Day Wave was positively correlated with sea surface temperature in the eastern, equatorial Pacific. He speculated that additional equatorial precipitation associated with warm phases of the El Nino–Southern Oscillation, was more efficient in exciting the 5-Day Wave. This would lead one to conclude that convective heating is an important part of the wave forcing. Miyoshi and Hirooka's (1999) experiment with a spectral GCM showed that the largest difference in the 5-Day Wave was between a control and a dry simulation further supporting this conclusion.

Horinouchi and Yoden (1996) found that one of the dominant responses to localized heating in the tropics was the excitation of free modes in their theoretical study with a linearized primitive equation model. They noted that heating off the equator was more effective in exciting Rossby waves than heating on the equator. They were cautious in assuming that their results could be directly applied to the real atmosphere primarily because the aforementioned contrasting conclusions of Manzini and Hamilton (1993).

Although some combination of these random forcing seem to be adequate to explain the excitation of free Rossby waves, other mechanisms besides direct forcing by mountain and heat sources have been proposed. Farrell (1988) showed that free waves could draw on mean flow energy for their excitation given a favourable initial perturbation. Da Silva and Lindzen (1987) proposed that adjustment of the quasi-stationary forced waves to changing zonal winds excited transients that corresponded to the gravest free modes.

Forcing of free waves is undoubtedly complex and varied and, overtime, each of these mechanisms may play roles.

9. Summary

Free Rossby waves of small $\boldsymbol{s}$ and $\boldsymbol{l}$ are evident in the 40-yr record of NCEP/NCAR Reanalysis data studied here. Wave modes with $\boldsymbol{l} < 4$ are easiest to detect and they look very much like their theoretical prototypes. Although the threshold is variable, modes roughly with $\boldsymbol{l} > 4$ are distorted considerably by the background flow, often do not exist as discrete modes, and they are difficult to unambiguously detect when they do. Identifiable modes sometimes have large amplitudes and contribute a sizeable amount to the total variance. Seasonal variations are not particularly large although there is a tendency for wave activity to be stronger in the northern winter.

Free waves have been related to blocking episodes and to time variations in transport of atmospheric properties. It has been proposed that they affect Earth orientation values. Although the published evidence is convincing, more research is still needed to fully understand these effects of free Rossby waves.

Free Rossby waves have been found in a series of models. This is not surprising since models are built on the equations that predict them. Of particular importance were the difficulties they posed for early numerical forecast models. The excitation of spurious free Rossby waves were documented to cause large

errors in the prediction of the long waves that were unexpected from predictability theory. The remarkable improvement of forecasts over that time attests to the ever improving fidelity of our numerical weather forecast models, but it would be important to determine if there is any need left to improve the handling of free Rossby waves. It might be good for us to better observe how, where, and when waves are excited so we can better anticipate their influences on the large-scale flow.

Rossby wave dynamics are at the core of dynamic meteorology. Free Rossby waves represent rare phenomena that were predicted by theory before they were observed in nature. Although they have engendered considerable attention in the literature, that attention has waned in the recent decade. We hope that this update will reinvigorate interest that will lead to an increase in our understanding of large-scale variations in the atmospheric, and possibly some in the oceans and in Earth orientation variables as well.

10. Acknowledgments

I thank A. Kasahara for encouragement and for the use of his code to compute Hough functions. R. Valent gave me a version that would run on my machine. G. Branstator and A. Mai provided their stream function data. J. Tribbia had answers to many of my questions. T. Hollingsworth's comments helped me to better understand current forecast performance. H. Hendon and M. Salby provided thorough reviews of an earlier version of the paper. T. Hoar and A. Phillips gave advice on MATLAB and the WEB. Some of the work was done at Scripps Institution of Oceanography and the U. of Hawaii, and I thank D. Cayan, Climate Research Division at Scripps and B. Wang, International Pacific Research Center and the Department of Meteorology at Hawaii, for their hospitality.

References

Ahlquist, J. 1982. Normal-mode global Rossby waves: theory and observations. *J. Atmos. Sci.* **39**, 193–202.

Ahlquist, J. 1985. Climatology of normal-mode Rossby waves. *J. Atmos. Sci.* **42**, 2059–2068.

Barnett, T. P. 1983. Interaction of the monsoon and Pacific trade wind system at interannual time scales. Part I: the equatorial zone. *Mon. Wea. Rev.* **111**, 756–773.

Branstator, G. 1987. A striking example of the atmosphere's leading traveling pattern. *J. Atmos. Sci.* **44**, 2310–2323.

Branstator, G. and Held, I. 1995. Westward propagating normal modes in the presence of stationary background waves. *J. Atmos. Sci.* **52**, 247–262.

Branstator, G. and Fredricksen, J. 2003. The seasonal cycle of interannual variability and the dynamical imprint of the seasonally varying mean state. *J. Atmos. Sci.* **60**, 1577–1592.

Burpee, R. W. 1976. Some features of global-scale 4–5 day waves. *J. Atmos. Sci.* **33**, 2292–2299.

Charney, J. G. and Eliassen, A. 1949. Anumerical method for predicting the perturbations of the middle latitude westerlies. *Tellus* **1** (2), 38–54.

Cheong, H.-B. and Kimura, R. 1997. Excitation of the 5-Day wave by Antarctica. *J. Atmos. Sci.* **54**, 87–102.

Cheong, H.-B. and Kimura, R. 2001. Excitation of the 10-Day and 16-Day waves. *J. Atmos. Sci.* **58**, 1129–1145.

Clark, J. H. E. 1972. The vertical propagation of forced atmospheric planetary. *J. Atmos. Sci.* **29**, 1430–1473.

Cressman, G. P. 1958. Barotropic divergence and very long atmospheric waves. *Mon. Wea. Rev.* **86**, 293–297.

Daley, R. and Williamson, D. L. 1985. The existence of free Rossby waves during January 1979. *J. Atmos. Sci.* **42**, 2121–2141.

Daley, R., Tribbia, J. and Williamson, D. L. 1981. The excitation of large-scale free Rossby waves in numerical weather prediction. *Mon. Wea. Rev.* **109**, 1836–1861.

Da Silva, A. and Lindzen, R. S. 1987. A mechanism for excitation of ultralong Rossby waves. *J. Atmos. Sci.* **44**, 3625–3639.

Deland, R. 1964. Traveling planetary waves. *Tellus* **16**, 271–273.

Diky, L. A. 1965. The terrestrial atmosphere as an oscillating system. *Izv. Atmos. Ocean Phys.* **1**, 275–286.

Diky, L. A. and Golitsyn, G. S. 1968. Calculation of the Rossby wave velocities in the Earth's atmosphere. *Tellus* **20**, 314–317.

Elbern, H. and Speth, P. 1993. Energy of Rossby waves as part of global atmospheric oscillations. *Tellus* **45A**, 168–192.

Eliasen, E. and Machenhauer, B. 1965. A study of the fluctuations of atmospheric planetary flow patterns represented by spherical harmonics. *Tellus* **17**, 220–238.

Eliasen, E. and Machenhauer, B. 1969. On the observed large-scale atmospheric wave motions. *Tellus* **21**, 149–165.

Eubanks, T. M., Steppe, J. A., Dickey, J. O., Rosen, R. D. and Salstein, D. A. 1988. Causes of rapid motinons of the Earth's pole. *Nature* **134**, 115–119.

Farrell, B. 1988. Optimal excitation of neutral Rossby waves. *J. Atmos. Res.* **45**, 163–172.

Ferranti, L., Klinker, E., Hollingsworth, A. and Hoskins, B. J. 2002. Diagnosing of systematic forecast errors dependent on flow pattern. *Q. J. R. Meteorol. Soc.* **128**, 1623–1640.

Forbes, J. M., Hagan, M. E., Miyahara, S., Vial, F., Manson, A. H. and co-authors. 1995. Quasi 16-Day oscillation in the mesosphere and lower thermosphere, J. *Geophys. Res.* **100**, 9149–9163.

Garcia, R. R. and Geisler, J. E. 1981. Stochasic forcing of small-amplitude oscillations in the stratosphere. *J. Atmos. Sci.* **38**, 2187–2197.

Garcia, R. R. and Salby, M. L. 1987. Transient response to localized episodic heating in the tropics. Part II: far-field behavior. *J. Atmos. Sci.* **44**, 499–530.

Geisler, J. E. 1974. A numerical model of the sudden stratospheric warming mechanism. *J. Geophys. Res.* **79**, 4989–4999.

Geisler, J. E. and Dickinson, R. E. 1975. External Rossby modes on a β-plane with realistic vertical wind shear. *J. Atmos. Sci.* **32**, 2082–2093.

Hamilton, K. 1985. A possible relationship between tropical ocean temperatures and the observed amplitude of the atmospheric (1,1) Rossby normal mode. *J. Geophys. Res.* **90**, 8071–8074.

Hamilton, K. 1987. General circulation model simulation of the structure and energetics of atmospheric normal modes. *Tellus* **39A**, 435–459.

Haurwitz, B. 1940. The motion of atmospheric diturbances on the spherical earth. *J. Mar. Res.* **3**, 254–267.

Hayashi, Y. 1974. Spectral analysis of tropical disturbances appearing in a GFDL general circulation model. *J. Atmos. Sci.* **31**, 180–218.

Hayashi, Y. 1981. Space-time cross spectral analysis using the maximum entropy method. *J. Meteor. Soc. Japan,* **54**, 620–624.

Hayashi, Y. and Golder, D. G. 1983. Transient planetary waves simulated by GFDL spectral general circulation models. *Part 1: effects of mountains. J. Atmos. Sci.* **40**, 941–950.

Heckley, W. A. and Gill, A. E. 1984. Some simple analytical solutions to the problem of forced equatorial long waves. *Q. J. R. Meteorol. Soc.* **110**, 203–217.

Hirooka, T. 1986. Influence of normal mode Rossby waves on the mean field: interference with quasistationary waves. *J. Atmos. Sci.* **43**, 2088–2097.

Hirooka, T. 2000. Normal mode Rossby waves as revealed by UARS/ISAMS observations. *J. Atmos. Sci.* **57**, 1277–1285.

Hirooka, T. and Hirota, I. 1985. Normal mode Rossby waves observed in the upper stratosphere. Part II: second antisymetric modes of zonal wave numbers 1 and 2. *J. Atmos. Sci.* **42**, 536–548.

Hirooka, T. and Hirota, I. 1989. Further evidence of normal mode Rossby waves. *Pure Appl. Geophys.* **130**, 277–289.

Hirota, I. 1971.Excitation of planetary Rossby waves in the winter stratosphere by periodic forcing. *J. Meteor. Soc. Japan* **49**, 439–449.

Hirota, I. and Hirooka, T. 1984. Normal mode Rossby waves observed in the upper stratosphere. Part I: first symmetric modes of zonal wavenumber 1 and 2. *J. Atmos. Sci.* **41**, 1253–1267.

Hollingsworth, A., Arpe, K., Tiedtke, M., Capaldo, M. and Savijärvi, H. 1980. The performance of a medium-range forecast model in winter – impact of physical parameterizations. *Mon. Wea. Rev.* **108**, 1736–1773.

Horel, J. D. 1984. Complex principal component analysis: theory and examples. *J. Clim. Appl. Meteor.* **23**, 1660–1673.

Horinouchi, T. and Yoden, S. 1996. Excitation of transient waves by localized episodic heating in the tropics and their propagation into the middle atmosphere. *J. Meteor. Soc. Japan* **74**, 189–210.

Hough, S. S. 1898. On the application of harmonic analysis o the dynamical theory of tides, II, on the general integration of Laplace's dynamical equations. *Phil. Trans. Roy. Soc. Lond., Ser. A* **191**, 139–185.

Jenkins, G. M. and Watts, D. G. 1968. *Spectral Analysis and its Applications*. Holden-Day, San Francisco, 525pp.

Julian, P. R. 1975. Comments on the determination of significance levels of the coherence statistic. *J. Atmos. Sci.* **32**, 836–837.

Kalnay, E. and co-authors 1996. The NCEP/NCAR 40-year Reanalysis Project. *Bull. Amer. Meteor. Soc.* **77**, 437–471.

Kasahara, A. 1976. Normal modes of ultralong waves in the atmosphere. *Mon. Wea. Rev.* **104**, 669–690.

Kasahara, A. 1980. Effect of zonal flows on the free oscillations of a barotropic atmosphere. *J. Atmos. Sci.* **37**, 917–929.

Kubota, S. and Iida, M. 1954. Statistical characteristics of atmospheric disturbances. *Pap. Meteorol. Geophys.* **5**, 22–34.

Kushnir, Y. 1987. Retrograding winter time low-frequency disturbance over the North Pacific Ocean. *J. Atmos. Sci.* **44**, 2727–2742.

Lamb, H. H. 1932. *Hydrodynamics, Dover, NY,* 738pp.

Lambert, S. J. and Merilees, P. E. 1978. A study of planetary wave errors in a spectral numerical prediction model. *Atmos. Oceans* **16**, 197–211.

Lejenäs, H. and Döös, B. R. 1987. The behavior of the stationary and traveling planetary-scale waves during blocking—a northern hemisphere data study. *J. Meteor. Soc. Japan* **65**, 709–725.

Lejenäs, H. and Madden, R. A. 1992. Traveling planetary-scale waves and blocking. *Mon. Wea. Rev.* **120**, 2821–2830.

Lejenäs, H. and Madden, R. A. 2000. Mountain torques caused by normal-mode global Rossby waves, and the impact on atmospheric angular momentum. *J. Atmos. Sci.* **57**, 1045–1051.

Lindzen, R. S. 1967. Planetary waves on β planes. *Mon. Wea. Rev.* **95**, 441–451.

Lindzen, R. S. 1986. Stationary planetary waves blocking, and interannual variability, *in Advances in Geophysics* **29**, 251–273. Academic Press, London.

Lindzen, R. S., Farrell, B. and Jacqmin, D. 1982. Vacillations due to wave interference: applications to the atmosphere and to annulus experiments. *J. Atmos. Sci.* **39**, 14–23.

Lindzen, R. S., Straus, D. M. and Katz, B. 1984. An an observational study of large-scale atmospheric Rossby waves during FGGE. *J. Atmos. Sci.* **41**, 1320–1335.

Longuet-Higgins, M. S. 1968. The eigenfunctions of Laplace's tidal equations over a sphere. *Phil. Trans. Roy. Soc. Lond., Ser. A* **262**, 511–607.

Lorenz, E. N. 1969. The predictability of flow which contains many scales of motion. *J. Atmos. Sci.* **21**, 289–307.

Madden, R. A. 1975. Oscillations in the winter stratosphere. Part 2: the role of horizontal eddy heat transport and the interaction of transient and stationary planetary-scale waves. *Mon. Wea. Rev.* **103**, 717–729.

Madden, R. A. 1978. Further evidence of traveling planetary waves. *J. Atmos. Sci.* **35**, 1605–1618.

Madden, R. A. 1979. Observations of large-scale traveling Rossby waves. *Rev. Geophys. Space Phys.* **17**, 1935–1949.

Madden, R. A. 1983. The effect of the interference of traveling and stationary waves on time variations of the large-scale circulation. *J. Atmos. Sci.* **40**, 1110–1125.

Madden, R. A. and Labitzke, K. 1981. A free Rossby wave in the troposphere and stratosphere during January 1979. *J. Geophys. Res.* **86**, 1247–1254.

Madden, R. A. and Speth, P. 1995. Estimates of the angular momentum, friction and mountain torques during 1987–1988. *J. Atmos. Sci.* **52**, 3681–3694.

Manzini, E. and Hamilton, K. 1993. Middle atmosphere traveling waves forced by latent and convective heating. *J. Atmos. Sci.* **50**, 2180–2200.

Margulis, M. 1893. Luftbewegungen in einer rotierended spharoidschale. *Sber, Akad. Wiss. Wien* **102**, 11–56 (in German).

McIntyre, M. E. and Palmer, T. N. 1983. Breaking planetary waves in the stratosphere. *Nature* **305**, 593–600

Miyoshi, Y. and Hirooka, T. 1999. A numerical experiment of excitation of the 5-Day wave by a GCM. *J. Atmos. Sci.* **56**, 1698–1707.

Palmer, T. N. 1981. Diagnostic study of a wavenumber-2 stratospheric sudden warming in a transformed Eulerian-mean formalism. *J. Atmos. Sci.* **38**, 844–855

Platzman, G. 1968. The Rossby wave. *Q. J. R. Meteorl. Soc.* **94**, 225–248.

Ponte, R. M. 1997. Nonequilibrium response of the global ocean to the 5-Day Rossby-Haurwitz wave in atmospheric surface pressure. *J. Phys. Ocean.* **27**, 2158–2168.

Quiroz, R. 1987. Traveling waves and regional transitions in blocking activity in the Northern Hemisphere. *Mon. Wea. Rev.* **115**, 919–935.

Rossby, C.-G. 1949. On the dispersion of planetary waves in a barotropic atmosphere. *Tellus* **1**, 54–58.

Rossby, C.-G., *et al*. 1939. Relations between variations in the intensity of the zonal circulationof the atmosphere and the displacements of the semipermantent centers of action. *J. Mar. Res.* **2**, 38–55.

Salby, M. L. 1981a. Rossby normal modes in nonuniform background configurations. Part I: simple nonuniformities. *J. Atmos. Sci.* **38**, 1803–1826.

Salby, M. L. 1981b. Rossby normal modes in nonuniform background configurations. Part II: equinox and solstice conditions. *J. Atmos. Sci.* **38**, 1827–1840.

Salby, M. L. 1981c. The 2-Day wave in the middle atmosphere: observations and theory. *J. Geophys. Res.* **86**, 9654–9660.

Salby, M. L. 1984. Survey of planetary-scale traveling waves: the theory and observations. *Rev. Geophys. Space Phys.* **22**, 209–236.

Salby, M. L. and Garcia, R. R. 1987a. Vacillation induced by interference of stationary and traveling planetary waves. *J. Atmos. Sci.* **44**, 2679–2711.

Salby, M. L. and Garcia, R. R. 1987b. Transient response to localized episodic heating in the tropics. Part II: far-field behavior. *J. Atmos. Sci.* **44**, 458–498.

Smith, A. K. 1985. Wave transience and wave-mean flow interaction caused by the interference of stationary and travaling waves. *J. Atmos. Sci.* **42**, 529–535

Speth, P. and Madden, R. A. 1983. Space-time spectral analyses of Northern Hemisphere geopotential heights. *J. Atmos. Sci.* **40**, 1086–1100.

Tsay, C.-Y. 1974. Analysis of large-scale wave disturbances in the tropics simulated by an NCAR general circulation model. *J. Atmos. Sci.* **31**, 330–339.

Venne, D. E. 1989. Normal-Mode Rossby waves observed in the wavenumber 1–5 geopotential fields of the stratosphere and troposphere. *J. Atmos. Sci.* **46**, 1042–1056.

Vincent, R. A. 1984. MF/HF radar measurements of the dynamics of the mesopause region – a review. *J. Atmos. Terr. Phys.* **46**, 961–974.

von Storch, H. and Zwiers, F. W. 1999. *Statistical Analysis in Climate Research*, Cambridge University Press, Cambridge, 484pp.

Wallace, J. M. and Dickinson, R. E. 1972. Empirical orthogonal representation of time series in the frequency domain. *Part I: theoretical considerations. J. App. Meteor.* **11**, 887–892.

Wallace, J., Tibaldi, S. and Simmons, A. J. 1983. Reduction of systematic forecast errors in the ECMWF model throughthe introduction of an envelope orography. *Q. J. R. Meteorol. Soc.* **109**, 683–917.

Weber, R. O. and Madden, R. A. 1993. Evidence of traveling external Rossby waves in the ECMWF analyses. *J. Atmos. Sci.* **50**, 2994–3007.

Wolff, P. M. 1958. The error in numerical forecasts due to retrogression of the ultra-long waves. *Mon. Wea. Rev.* **86**, 245–250.